Device-Parameter Estimation with On-chip Variation Sensors Considering Random Variability

Ken-ichi Shinkai*, Masanori Hashimoto*,

* Department of Information Systems Engineering, Osaka University, Osaka, Japan
Email: {shinkai.kenichi, hasimoto}@ist.osaka-u.ac.jp

***Abstract*—Device-parameter monitoring sensors inside a chip are gaining its importance as the post-fabrication tuning is becoming of a practical use. In estimation of variational parameters using on-chip sensors, it is often assumed that the outputs of variation sensors are not affected by random variations. However, random variations can deteriorate the accuracy of the estimation result. In this paper, we propose a device-parameter estimation method with on-chip variation sensors explicitly considering random variability. The proposed method derives the global variation parameters and the standard deviation of the random variability using the maximum likelihood estimation. We experimentally verified that the proposed method can accurately estimate variations, whereas the estimation result deteriorates when neglecting random variations. We also demonstrate an application result of the proposed method to test chips fabricated in a 65-nm process technology.**

***Index Terms*—variation sensor, device-parameter extraction, process variability, die-to-die variation, within-die variation**

I. Introduction

Process variability is becoming more influential on circuit performance and is predicted to be severer further in the future [1]. The process variability is often classified into D2D (Die-to-Die) and WID (WithIn-Die) variations. Especially, WID variation has been predicted to become more significant as technology advances [2].

To improve the circuit performance after fabrication, several compensation methods, such as adaptive body bias and voltage scaling, have been proposed [3], [4]. In order to compensate the performance efficiently, we have to estimate for each chip how device-parameters varied from their typical values during manufacturing. I-V curve measurement is a popular approach to obtain characteristics of each transistor [5]–[8]. However, I-V curve measurement requires an analog voltage and a current measurement equipment. Therefore, it is adopted for precise process characterization, but it is not suitable for estimating device-parameters for each chip aiming at chip by chip performance compensation.

On the other hand, RO(Ring-Oscillator)-based sensors have been intensively studied [9]–[12]. They can be easily implemented on a chip and can be used to obtain variability information even after the product shipment because the oscillating frequencies of ROs can be easily measured. Conventional device-parameter extraction methods using RO-based sensors often assume that ROs are not affected by random variations because of the well-known averaging effect, that is the influence of random variation is assumed to be well suppressed by increasing the number of stages [13].

ROs that have high-sensitivity to a single device-parameter have been proposed for decomposing the measured superposed variation into each device-parameter variation [10], [12]. However, when using such ROs, random variations might not be canceled out. An example is shown in Fig. 1. Here, the number of RO stages is 101. The condition of this experiment is basically the same as that in the following sections, and will be explained later. ΔF denotes the shift of the oscillation frequency in a RO from its nominal value. Random variations of $\Delta V_{th_{n/p}}$ and $\Delta L_{n/p}$, whose averages are 0, are given, where $V_{th_{n/p}}$ means N/PMOS threshold voltage and $L_{n/p}$ is gate length of N/PMOS. When a RO is composed of normal inverters, the average of ΔF is shifted by -1.43% and the standard deviation is 1.23%. On the other hand, when a RO consists of sophisticated inverters that have intentionally high-sensitivity to a device-parameter of ΔVth_n, the effect of random variability on ΔF is more significant. In fact, the random variability changes the average of ΔF by -10.8% even though the averages of every variation are 0. The standard deviation reaches 3.83% indeed. Therefore, in order to accurately estimate device-parameters using such sophisticated ROs, we should take into account random variability explicitly. Both the large standard deviation of ΔF and the shift of the average must be considered in the device-parameter estimation from the measured sensor outputs.

In this paper, we propose an estimation method of device-parameters, such as threshold voltage V_{th} and channel-length

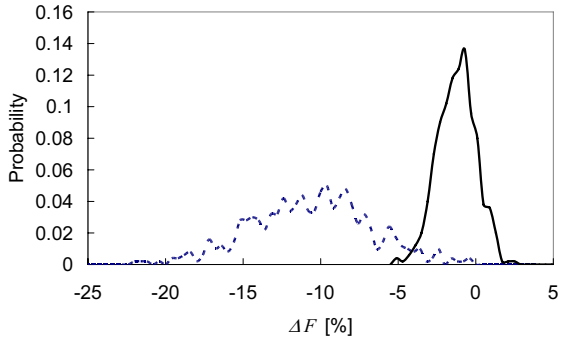

Fig. 1. Frequency-distributions with only random variations (without global variations) . For each distribution, the number of sampled data is 500. Supply voltage is 0.9 V. Solid line denotes a distribution with a RO constructed by normal inverters (RO#1 in Section IV-A), and dashed line denotes that with a RO constructed by inverters that have high-sensitivity to NMOS V_{th} (RO#2 in Section IV-A)). The number of stages in both ROs is 101.

978-1-4244-7514-8/11/$26.00 ©2011 IEEE

L of a transistor, explicitly considering the effect of random variability. We obtain the variability information by using some RO variation sensors whose frequency-sensitivity vectors to parameter variation are orthogonal. We then estimate device-parameters by MLE (Maximum Likelihood Estimation).

The rest of this paper is organized as follows. Section 2 explains RO-based variation sensor. Section 3 describes the proposed method to extract device-parameters considering random variability. The proposed method is experimentally validated in Section 4. We apply the proposed method to test chips in Section 5, and the discussion is concluded in Section 6.

II. RO-BASED VARIATION SENSOR

In this paper, it is assumed that the variability is composed of two components, that are global and random variations*. Global is D2D variation which causes the same variation-offset to all transistors on a chip, while random is WID variation which is different transistor by transistor. Thus, an offset of device-parameter x from its nominal value, ΔV_x, is expressed by Eq. (1),

$$\Delta V_x = \Delta G_x + \Delta R_x, \tag{1}$$

where G denotes global variability, and R corresponds to random variability.

In this paper, we use several RO variation sensors whose structures are different and estimate ΔG_x and the standard deviation of ΔR_x of several device-parameters from the measured oscillating frequencies, whereas conventional methods assume ΔR_x is ignorable.

A. Conventional parameter estimation method using RO-based variation sensors

A conventional parameter estimation method assumes that the shift of the oscillation frequency in the i-th type of RO from its nominal value, ΔF_i, is expressed by Eq. (2),

$$\Delta F_i = \sum_x k_{xi} \Delta G_x = \boldsymbol{k_{xi}}^{\mathrm{T}} \boldsymbol{\Delta G_x}, \tag{2}$$

where k_{xi} denotes the frequency-sensitivity to the variation of parameter x at RO#i. $\boldsymbol{k_{xi}}$ and $\boldsymbol{\Delta G_x}$ are vector representations of k_{xi} and ΔG_x. Note that Eq. (2) can be extended to quadratic or higher-order model to improve the accuracy [14]. In this model, random variations are assumed to be canceled out and much smaller than the global variation because of the averaging effect. Therefore, none of ΔR_x appear in Eq. (2). Using Eq. (2), device-parameter variations can be estimated by Eq. (3).

$$\boldsymbol{\Delta G_x} = \begin{pmatrix} \boldsymbol{k_{x1}}^{\mathrm{T}} \\ \vdots \\ \boldsymbol{k_{xn}}^{\mathrm{T}} \end{pmatrix}^{-1} \boldsymbol{\Delta F}. \tag{3}$$

*Other variability components, such as spatially-correlated component, could be expected to be estimated by modifying the maximum likelihood estimation in Section III, but it will not be discussed further in this paper.

At least n ROs should be used for the estimation of n parameters.

B. RO design using frequency-sensitivity vectors

To estimate each device-parameter accurately, carefully choosing a set of RO sensors is important. The sensitivity vectors of RO sensors, which corresponds to $\boldsymbol{k_{xi}}$ in Eq. (3), should be orthogonal [10], [12], [14]. If all the sensitivity vectors are orthogonal to each other, the estimation result of $\boldsymbol{\Delta G_x}$ becomes more accurate. We determine an effective set of ROs so that RMSE (Route Mean Square Error) of degrees in Eq. (4) is minimized.

$$RMSE(ROset) = \sqrt{\frac{\sum_{\forall i \in (ROset)} \sum_{\forall j \in (ROset), j \neq i} (degree_{ij} - 90^\circ)^2}{{}_n\mathrm{C}_2}}, \tag{4}$$

where $ROset$ is the set of ROs used for parameter estimation and the number of ROs in $ROset$ is n. $degree_{ij}$ denotes the degree between the sensitivity vectors of RO#i and RO#j.

III. METHOD TO EXTRACT DEVICE-PARAMETERS USING MAXIMUM LIKELIHOOD ESTIMATION

The device-parameter estimation in Eq. (3) assumes that ΔR_x can be suppressed to be ignorable. However, as shown in Fig. 1, the assumption is difficult to be valid. The necessary number of RO stages is very large, which consumes large silicon area. This section presents the proposed method to estimate device-parameters from the sensor outputs that include random variability.

Fig. 2 illustrates that the probability density function of ΔF_i changes according to $\boldsymbol{\Delta G_x}$ and $\boldsymbol{\sigma_{\Delta R_x}}$, where $\sigma_{\Delta R_x}$ is the standard deviation of ΔR_x. Here, let us suppose that the probability density function is expressed by a normal distribution, namely the distribution of the measured ΔF_i follows $\mathrm{N}(\mu_{\Delta F_i}, \sigma^2_{\Delta F_i})$, although other distributions can be assumed. We estimate $\boldsymbol{\Delta G_x}$ and $\boldsymbol{\sigma_{\Delta R_x}}$ using MLE in the following.

Conventionally, $\mu_{\Delta F_i}$ is assumed to be a function of only $\boldsymbol{\Delta G_x}$ described by Eq. (5),

$$\mu_{\Delta F_i} = f(\boldsymbol{\Delta G_x}). \tag{5}$$

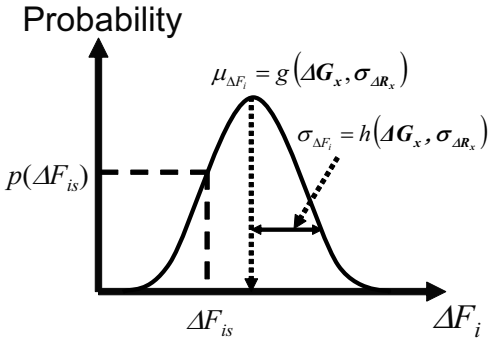

Fig. 2. Probability density function used for maximum likelihood estimation.

However, Eq. (5) is not sufficient to estimate device-parameters accurately, especially when dedicated high-sensitive ROs are used as pointed out in Fig. 1. Instead of Eq. (5), we model ΔF_i in a chip as a normal distribution $\mathrm{N}(\mu_{\Delta F_i}, \sigma^2_{\Delta F_i})$, as expressed in Eqs. (6) and (7).

$$\mu_{\Delta F_i} = g(\boldsymbol{\Delta G_x}, \boldsymbol{\sigma_{\Delta R_x}}), \tag{6}$$

$$\sigma_{\Delta F_i} = h(\boldsymbol{\Delta G_x}, \boldsymbol{\sigma_{\Delta R_x}}). \tag{7}$$

We can freely choose the base and order of functions $g(\boldsymbol{\Delta G_x}, \boldsymbol{\sigma_{\Delta R_x}})$ and $h(\boldsymbol{\Delta G_x}, \boldsymbol{\sigma_{\Delta R_x}})$ according to the required accuracy. If we choose the first-order approximation, for example, they are expressed by Eqs. (8) and (9),

$$\mu_{\Delta F_i} = \sum_x \left(a_{xi} \Delta G_x + b_{xi} \sigma_{\Delta R_x} \right), \tag{8}$$

$$\sigma_{\Delta F_i} = \sum_x \left(c_{xi} \Delta G_x + d_{xi} \sigma_{\Delta R_x} \right), \tag{9}$$

where $a/b/c/d_{xi}$ are coefficients.

Eq. (10) shows the probability density function of ΔF_i,

$$p(\Delta F_i) = \frac{1}{\sqrt{2\pi}\sigma_{\Delta F_i}} \, exp\left(-\frac{(\Delta F_i - \mu_{\Delta F_i})^2}{2\sigma^2_{\Delta F_i}} \right). \tag{10}$$

Note that the presented estimation method is independent of the shape of the assumed distribution. When there are S_i sensors of RO#i on a chip, the likelihood function of ΔF_i is expressed by Eq. (11),

$$\prod_s^{S_i} p(\Delta F_{is}) = \prod_s^{S_i} \frac{1}{\sqrt{2\pi}\sigma_{\Delta F_i}} \, \exp\left(-\frac{(\Delta F_{is} - \mu_{\Delta F_i})^2}{2\sigma^2_{\Delta F_i}} \right), \tag{11}$$

where ΔF_{is} means measured data from the s-th sensor instance of the i-th type of RO. When we use n types of ROs for estimation, the overall likelihood function becomes Eq. (12). We find $\boldsymbol{\Delta G_x}$ and $\boldsymbol{\sigma_{\Delta R_x}}$ that maximize Eq. (12), which are the device-parameters we want to estimate in this paper.

$$\prod_i^n \prod_s^{S_i} p(\Delta F_{is}). \tag{12}$$

The logarithm of Eq. (12) is expressed as Eq. (13), and The maximization of Eq. (13) is often easier to perform.

$$\sum_i^n \sum_s^{S_i} \log(p(\Delta F_{is}))$$
$$= -\frac{\log 2\pi \sum_i^n S_i}{2} - \frac{\sum_i^n S_i \log \sigma^2_{\Delta F_i}}{2} - \frac{1}{2} \sum_i^n \sum_s^{S_i} \left(\frac{(\Delta F_{is} - \mu_{\Delta F_i})^2}{\sigma^2_{\Delta F_i}} \right). \tag{13}$$

IV. Validation of the Proposed Extraction Method

In this section, we experimentally validate the proposed extraction method using virtually-fabricated chips (simulated data).

A. Experimental condition

As candidates for various ROs, we chose eight ROs listed in TABLE I to evaluate sensitivity vectors. Diagrams of these circuit are illustrated in Appendix. The number of stages in all ROs is 101. Structures of RO#2–3 and RO#4–8 are similar with those in [12] and [10], respectively. The difference between RO#4 and RO#5 is sizes of each transistor. RO#8 in Fig. 15 consists of an inverting stage in the modified L-sensitive RO in [10] (Fig. 14 in Appendix), while we customized it (Fig. 15 in Appendix) in order that four terminals (INVN/P and CAPN/P) are controllable to change the sensitivity vector. The experiment here assumes that selectable voltages at each terminal are V_{dd}, V_{bn}, V_{bp}, and V_{ss}, where V_{bn} and V_{bp} are generated by bias generators [10]. Therefore, we can obtain 144 ($= 3^2 4^2$) data only using RO#8. The oscillating frequency of every RO could be measured at different V_{dd}s. The sensitivity vectors vary depending on V_{dd}, which means we can increase the number of ROs without increasing the silicon area for sensors. In this paper, 1.5, 1.2, and 0.9 V are used as V_{dd}.

The combinations of ROs that can achieve the best and worst RMSE in Eq. (4) are shown in TABLE II. The best RMSE is 8.60° and the worst is 89.3°.

In what follows, we assume that $\sigma_{\Delta G_{Vth_{n/p}}}$=$\sigma_{\Delta R_{Vth_{n/p}}}$=35 mV and $\sigma_{\Delta G_{L_{n/p}}}$=$\sigma_{\Delta R_{Vth_{n/p}}}$=1 nm, unless otherwise stated. According to the assumed process variability, we virtually fabricated chips using Monte Carlo approach, and evaluated all sensors outputs with HSPICE. Here, each chip has 100 sensor instances for every type of ROs. We modeled Eqs. (5) and (6) as third-order polynomials, and Eq. (7) as second-order polynomials by fitting.

TABLE I
RO CONFIGURATION.

RO No.	Component
1	Normal INV
2	INV followed by NMOS transistor
3	INV followed by PMOS transistor
4	INV followed by CMOS-controlled load - 1
5	INV followed by CMOS-controlled load - 2
6	Current-starved INV followed by PMOS-controlled load [10]
7	Current-starved INV followed by NMOS-controlled load [10]
8	Customized INV

TABLE II
BEST AND WORST RO SETS. VOLTAGES ENCLOSED BY SQUARE BRACKETS AT RO#8 CORRESPOND TO INVN, INVP, CAPN, CAPP SHOWN IN FIG. 15.

RO No. (V_{dd})	RO No. (V_{dd})	RO No. (V_{dd})	RO No. (V_{dd})
2 (0.9)	8 (1.5) [V_{bn}, V_{bp}, V_{bn}, V_{ss}]	8 (1.5) [V_{bn}, V_{ss}, V_{dd}, V_{bn}]	8 (1.2) [V_{bp}, V_{bp}, V_{bp}, V_{bp}]
8 (0.9) [V_{bp}, V_{bp}, V_{bp}, V_{bn}]	8 (0.9) [V_{bp}, V_{bp}, V_{bp}, V_{bp}]	8 (0.9) [V_{bp}, V_{bp}, V_{bp}, V_{ss}]	8 (0.9) [V_{dd}, V_{bp}, V_{bp}, V_{ss}]

B. Under only global variations

We first evaluate the estimate accuracy when only global variations exist, i.e., $\sigma_{\Delta R_{Vth_{n/p}}} = \sigma_{\Delta R_{Vth_{n/p}}} = 0$. Thirty one chips were virtually fabricated. Eq. (5) is used for estimation.

TABLE III shows the averages of absolute estimation errors from the given variations. We verified that each global variation is accurately estimated when using the best RO set, while the worst RO set provides irrelevant estimation. Fig. 3 illustrates a scatter plot that compares estimated ΔG_{Vth_n} with those used in virtual fabrication. We can see that estimated parameters are consistent with the given parameters.

C. Under global and random variations

We evaluate the estimation accuracy when both global and random variations exist. Three chips were virtually fabricated. Eq. (6) and Eq. (7) are used for estimation, and we maximized Eq. (13) to obtain $\boldsymbol{\Delta G_x}$ and $\boldsymbol{\sigma_{\Delta R_x}}$. To resolve Eq. (13) in this experiment, we use the *optim* function of R [15] with L-BFGS (Limited-Broyden-Fletcher-Goldfarb-Shanno) algorithm.

1) Effect of random variability: First we demonstrate that neglecting random variability causes a significant degradation in accuracy. The proposed method is compared with the conventional one that uses only Eq. (5). Here we use the best RO set for both methods. TABLE IV shows the averages of the absolute estimation errors from the given variations. Excluding ΔG_{L_p}, all the results of the proposed method are improved. Our investigation shows that one of the reason why ΔG_{L_p} was not improved is that the second-order polynomials used for Eq. (7) is not sufficient to capture the non-linearity with regard to the parameters.

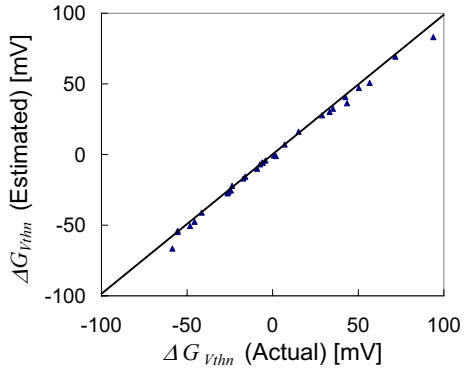

Fig. 3. Given $\Delta G_{V_{th_n}}$ vs. estimated $\Delta G_{V_{th_n}}$ under only global variations.

TABLE III
ABSOLUTE VALUES OF AVERAGE ESTIMATE ERRORS UNDER ONLY GLOBAL VARIATIONS (THE NUMBER OF VIRTUALLY-FABRICATED CHIPS IS 31).

RO set	ΔG_{Vth_n}[mV]	ΔG_{Vth_p}[mV]	ΔG_{L_n}[nm]	ΔG_{L_p}[nm]
Best	2.19	4.24	0.69	1.00
Worst	63.94	34.40	2.79	2.09

TABLE V lists the average absolute errors of estimated $\boldsymbol{\sigma_{\Delta R_x}}$. We assumed $\sigma_{\Delta R_{Vth_{n/p}}}$=35 mV and $\sigma_{\Delta R_{Vth_{n/p}}}$=1 nm, and the estimated results are correlated to them.

2) The importance of the number of sensors: We demonstrate how the number of sensor instances, i.e., S_i in Eqs. (11)–(13), affects the estimate accuracy. This evaluation is performed with the following process,

1) Make a set of sensor instances by randomly selecting those from 100 sensor instances on a virtually-fabricated chip,
2) Estimate variations using the above sensor set,
3) Go back to step 1 until a sufficient number of estimations are performed.

TABLE IV
ABSOLUTE VALUES OF AVERAGE ESTIMATE ERRORS UNDER GLOBAL AND RANDOM VARIATIONS (THE NUMBER OF VIRTUALLY-FABRICATED CHIPS IS THREE).

Method	ΔG_{Vth_n}[mV]	ΔG_{Vth_p}[mV]	ΔG_{L_n}[nm]	ΔG_{L_p}[nm]
Proposed	0.54	4.03	1.23	2.11
Conventional	8.51	13.71	1.49	0.54

TABLE V
AVERAGE ABSOLUTE ERRORS OF ESTIMATE OF $\boldsymbol{\sigma_{\Delta R_x}}$ (THE NUMBER OF VIRTUALLY-FABRICATED CHIPS IS THREE).

$\sigma_{\Delta R_{Vth_n}}$[mV]	$\sigma_{\Delta R_{Vth_p}}$[mV]	$\sigma_{\Delta R_{L_n}}$[nm]	$\sigma_{\Delta R_{L_p}}$[nm]
6.30	2.91	0.13	0.10

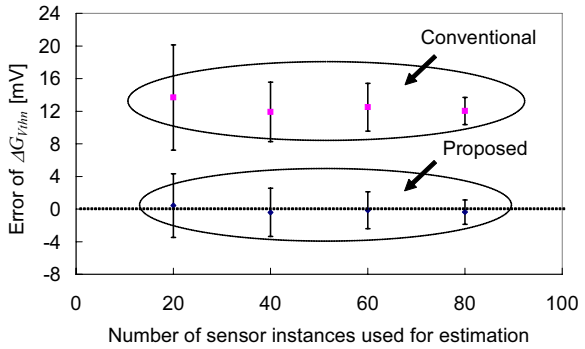

Fig. 4. The number of sensor instances vs. estimation error of $\Delta G_{V_{th_n}}$ (chip#2).

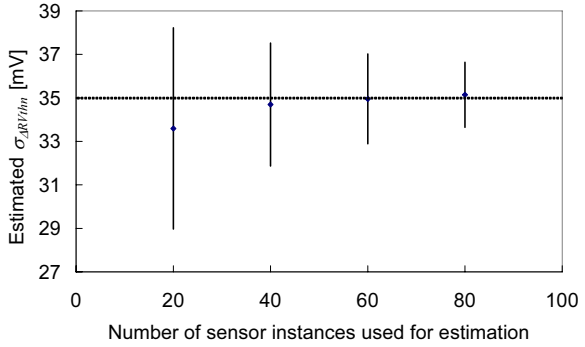

Fig. 5. The number of sensor instances vs. estimated $\sigma_{\Delta R_{V_{th_n}}}$ (chip#2).

We created 500 sets of sensor instances for this experiment. The number of sensor instances that we here evaluated are 20, 40, 60, and 80.

Fig. 4 illustrates the estimation result of $\Delta G_{V_{th_n}}$ at chip#2. Dots denote the average error, i.e., the expected value, in 500 sensor instances sets, and error bars show the standard deviation of the average error. More sensor instances are used, more accurate the estimation result is. The result of the conventional method denotes the same tendency of that of the proposed method. However, as the number of sensor instances decreases, the increasing rate in the standard deviation of conventional method is larger than that of the proposed method. Fig. 5 shows the estimation result of $\sigma_{\Delta R_{V_{th_n}}}$ in chip#2. Only the result with the proposed method is depicted, because the conventional method cannot estimate $\sigma_{\Delta R_{V_{th_n}}}$. If we want to suppress the error of $\mu_{\sigma_{\Delta R_x}} + 3\sigma_{\sigma_{\Delta R_x}}$ up to 20%, we need 60 sensor instances in a chip.

V. Test Chips in 65-nm Process

We designed test chips in a 65-nm process technology to verify the proposed method. The number of fabricated chips is 31.

A. Chip design

Fig. 7 illustrates the layout of the test chip. It has 84 sensor blocks, and each sensor block has eight ROs in TABLE I as shown in Fig. 8. Bias selector can output voltages to INVN/P and CAPN/P in Fig. 15, where selectable voltages are V_{dd}, V_{bn}, V_{bp}, and V_{ss}. V_{bn}/V_{bp} bias generators are implemented inside each sensor block. The oscillation frequency is measured by a 30-bit down counter implemented on the chip.

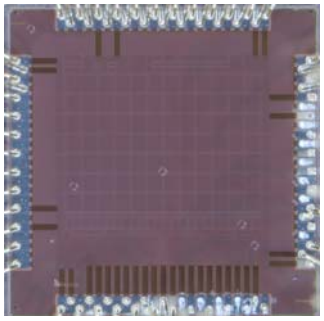

Fig. 6. Test chip in 65-nm process (chip size is 2.1 x 2.1 mm^2).

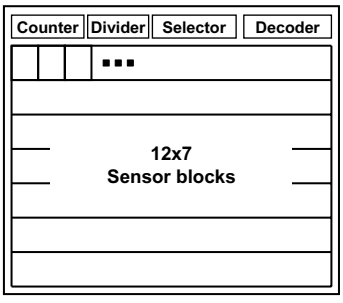

Fig. 7. Layout of chip.

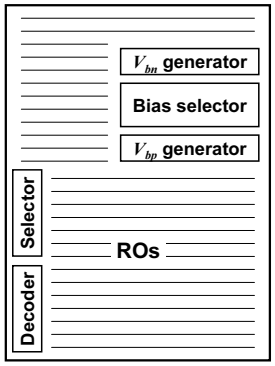

Fig. 8. Layout of sensor block.

B. Estimation example

We measured oscillation frequencies of the best RO set and estimated device-parameter variations using the proposed method. Here, we used all the sensors, i.e., 84 sensors, in a chip for the estimation. Fig. 9 shows the estimated $\sigma_{\Delta R_{V_{th_p}}}$ of each chip. Since the proposed method provides accuracy estimate as shown in Section IV-C, $\sigma_{\Delta R_{V_{th_p}}}$ in those chips is expected to be approximately within 25–40 mV. Further investigation on the measurement results is our future work.

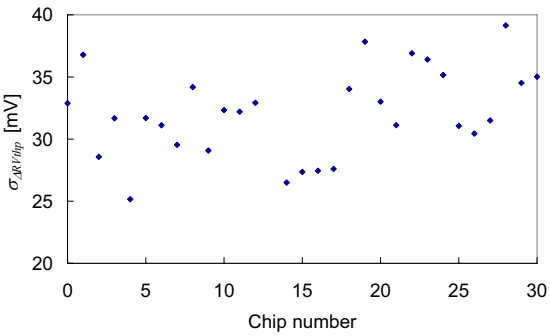

Fig. 9. Estimated $\sigma_{\Delta R_{V_{th_p}}}$.

VI. Conclusion

We proposed a device-parameter estimation method with on-chip variation sensors. The proposed method takes into account random variability with maximum likelihood estimation. We experimentally verified that the proposed method can accurately estimate variations, whereas disregarding random variability, which is often adopted in conventional methods, deteriorates the estimation accuracy of the global variation. We designed and fabricated test chips to validate the proposed method. Further study based on the measurement results of the test chips is our future work.

Acknowledgments

This work is supported by New Energy and Industrial Technology Development Organization (NEDO). The authors would like to thank VLSI Design and Education Center (VDEC), the University of Tokyo in collaboration with Synopsys, Inc. This work is also supported by Grant-in-Aid for Scientific Research and JSPS Fellows.

References

[1] H. Masuda, S. Ohkawa, A. Kurokawa, and M. Aoki, "Challenge: Variability Characterization and Modeling for 65- to 90-nm Processes," in *Proc. CICC*, 2005, pp. 593–599.

[2] H. Onodera, "Variability: Modeling and its impact on design," *IEICE Transactions on Electronics*, vol. 89, no. 3, pp. 342–348, 2006.

[3] S. Martin, K. Flautner, T. Mudge, and D. Blaauw, "Combined dynamic voltage scaling and adaptive body biasing for lower power microprocessors under dynamic workloads," in *Proceedings of the 2002 IEEE/ACM international conference on Computer-aided design*. ACM, 2002, pp. 721–725.

[4] J. Tschanz, J. Kao, S. Narendra, R. Nair, D. Antoniadis, A. Chandrakasan, and V. De, "Adaptive body bias for reducing impacts of die-to-die and within-die parameter variations on microprocessor frequency and leakage," *IEEE Journal of Solid-State Circuits*, vol. 37, no. 11, pp. 1396–1402, 2002.

[5] S. Ohkawa, M. Aoki, and H. Masuda, "Analysis and characterization of device variations in an LSI chip using an integrated device matrix array," *IEEE Transactions on Semiconductor Manufacturing*, vol. 17, no. 2, pp. 155–165, 2004.

[6] D. Fleury, A. Cros, K. Romanjek, D. Roy, F. Perrier, B. Dumont, H. Brut, and G. Ghibaudo, "Automatic extraction methodology for accurate measurements of effective channel length on 65-nm MOSFET technology and below," *IEEE Transactions on Semiconductor Manufacturing*, vol. 21, no. 4, pp. 504–512, 2008.

[7] K. Agarwal, J. Hayes, and S. Nassif, "Fast characterization of threshold voltage fluctuation in MOS devices," *IEEE Transactions on Semiconductor Manufacturing*, vol. 21, no. 4, pp. 526–533, 2008.

[8] S. Watabe, S. Sugawa, K. Abe, T. Fujisawa, N. Miyamoto, A. Teramoto, and T. Ohmi, "A Test Structure for Statistical Evaluation of Characteristics Variability in a Very Large Number of MOSFETs," in *IEEE International Conference on Microelectronic Test Structures*, 2009, pp. 114–118.

[9] M. Bhushan, M. Ketchen, S. Polonsky, and A. Gattiker, "Ring oscillator based technique for measuring variability statistics," in *2006 IEEE International Conference on Microelectronic Test Structures*, 2006, pp. 87–92.

[10] B. Wan, J. Wang, G. Keskin, and L. T. Pileggi, "Ring Oscillators for Single Process-Parameter Monitoring," in *Proc. Workshop on Test Structure Design for Variability Characterization*, 2008.

[11] L. Pang and B. Nikolic, "Measurements and Analysis of Process Variability in 90 nm CMOS," *IEEE Journal of Solid-State Circuits*, vol. 44, no. 5, pp. 1655–1663, 2009.

[12] I. A. K. M. Mahfuzul, A. Tsuchiya, K. Kobayashi, and H. Onodera, "Process-sensitive Monitor Circuits for Estimation of Die-to-Die Process Variability," in *Proc. TAU*, 2010, pp. 83–88.

[13] D. Blaauw, K. Chopra, A. Srivastava, and L. Scheffer, "Statistical Timing Analysis: From Basic Principles to State of the Art," *IEEE Transactions on CAD*, vol. 27, no. 4, pp. 589–607, 2008.

[14] T. Takahashi, T. Uezono, M. Shintani, K. Masu, and T. Sato, "On-die parameter extraction from path-delay measurements," in *IEEE Asian Solid-State Circuits Conference*, 2009, pp. 101–104.

[15] *R*. [Online]. Available: http://www.r-project.org/

APPENDIX

Appendix shows schematics of RO components described in TABLE I. Figs. 10–12 illustrate those of RO#2, RO#4 (5) and RO#6. RO#3 and RO#7 are exact complementary circuits of RO#2 and RO#6, respectively. V_{bn} bias generator is shown in Fig. 13 and it is complementary of V_{bp} bias generator. As described in Section IV-A, RO#8 in Fig. 15 is based on Fig. 14. Here we describes the characteristics of these circuits.

RO#2 component aims to be sensitive to variations in NMOS. RO#4 (5) component gains the sensitivity to L. When V_{thn} increases, the inverting stage slows down. However at that time, NMOS load becomes smaller due to the increased effective resistance of NMOS. The two behaviors cancel each other out and the fall-propagation delay is insensitive to V_{thn}. Similar discussion is applicable to V_{thp}. Therefore, when the devices are properly sized, this component can become either L_n- or L_p-sensitive.

V_{bn} bias generator provides the voltage that is inversely proportional to V_{thn} and less dependent of L_n. The description is omitted here because of space limitations, but it should be noted that L and W of transistors are very important to attain this property. Considering PMOS-loading effect and V_{bn} bias generator, RO#6 component mitigates L and V_{thp} variations, and enhances the sensitivity to V_{thn} variation.

The structure in Fig. 14 is modified from that in Fig. 11. The authors in [10] observed that the structure of Fig. 11 does not provide a sufficient cancellation of V_{th} variations in 65-nm devices. Thus, they combined structures of Figs. 11 and 12. They switched the bias voltages for N/PMOS and obtained the opposite cancellation/amplification effects for L and V_{th} variations. RO#8 component in Fig. 15 is similar with Fig. 14, while four terminals (INVN/P and CAPN/P) can be set to V_{dd}, V_{bn}, V_{bp}, and V_{ss} to change the sensitivity to variations.

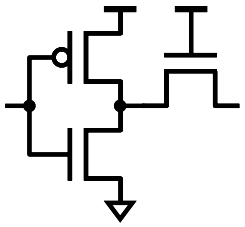

Fig. 10. RO#2 component: INV followed by NMOS transistor.

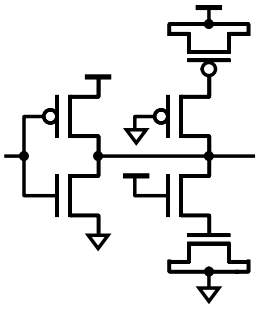

Fig. 11. RO#4 (5) component: INV followed by CMOS-controlled loads.

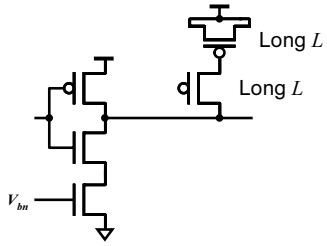

Fig. 12. RO#6 component: Current-starved INV followed by PMOS-controlled load.

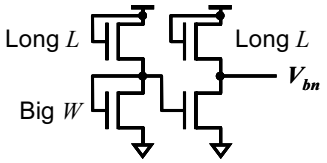

Fig. 13. V_{bn} bias generator for RO#6 and RO#8.

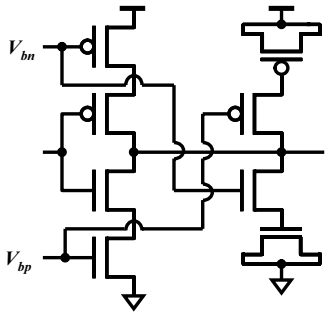

Fig. 14. Modified L-sensitive INV in [10].

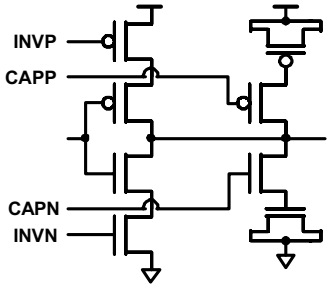

Fig. 15. RO#8 component: customized INV based on Fig. 14.